Progress in the pre-conceptual design of the auxiliary heating and current drive system for the Tokamak Energy Fusion Pilot Plant

Aleksandra Alieva*, *Nicolas* Lopez, *Steven* McNamara, *Yuichi* Takase, *Xin* Zhang, and TE FPP Team

Tokamak Energy LTD, 173 Brook Drive, Abingdon, UK, OX14 4SD

Abstract. Auxiliary heating and current drive is a crucial aspect of reactor-relevant tokamaks. Tokamak Energy is currently in the design phase of their Fusion Pilot Plant (FPP). Initial investigations for the flat-top phase of plasma scenarios rely exclusively on electron cyclotron (EC) waves as auxiliary heating and current drive source. This work focuses on parametric optimisation of the flat-top EC current drive scheme via ray-tracing simulations for three plasma scenarios, each having different magnetic field and aspect ratio. The purpose of the study is to maximise the normalised current drive efficiency ζ_{ECCD}. It is shown that EC waves in the O mode polarisation are capable of efficiently driving plasma current throughout the plasma volume, supporting the notion that EC waves can be the single auxiliary power source for flat-top operations.

1 Introduction

Tokamak Energy (TE) was selected to develop a pre-conceptual design of the Fusion Pilot Plant based on a spherical tokamak for the United States Department of Energy's (US DOE) Milestone-Based Fusion Development Program [1]. The purpose of this program is to support the development of fusion energy technology through a competitive, milestone-based approach. The duration is five years, divided over three budget periods. At the end of the first 18 months period, TE must provide a pre-conceptual design of the pilot plant.

The design of the TE FPP is based on a lower aspect ratio tokamak, as this is a promising candidate for a fusion reactor [2]. However, since the size of the central solenoid is limited in spherical tokamaks (ST), a non-inductive heating and current drive system has to be used to complement the inductive current drive. Electron-cyclotron resonance-based heating and current drive (HCD) is being considered because of the maturity of the technology and the advantages over other auxiliary HCD methods. The benefits are: good wave-plasma matching without attenuation of a vacuum wave to plasma (no evanescent region); no requirements for the large in-vessel plasma-facing components in the vicinity of the plasma edge (launchers take up relatively small space in breeding blanket). Moreover, flexibility in control of absorption and narrowness of power deposition profiles lead to good controllability of on- and off-axis HCD. This can benefit in current density profile tailoring enabling advance performance of tokamaks [3].

The design of the TE FPP has a high-temperature superconducting (HTS) solenoid to aid ramp-up, ramp-down, and potentially flat-top phases. This gives the machine the highest flexibility and adaptability to different physics scenarios. For the purpose of this work, the study focuses on a steady-state flat-top scenarios where the inductively driven current fraction is absent. As a result, it is crucial to analyse the propagation and absorption of EC waves and study the possibility of EC current drive (ECCD), as it, together with the bootstrap current, defines large parts of the plasma performance. The overall aim of the work is to find the maximum normalised ECCD efficiency ζ_{ECCD}, analyse and highlight the found trends. The paper is organised as follows. Plasma designs are introduced in Section 2. Section 3 presents the setup of the ECCD parametric scan. The results and discussion are given in Section 4. Finally, Section 5 summarises this study.

2 Plasma designs

The plasma design spaces were obtained using an integrated modelling workflow. The workflow scheme is presented in figure 1. There are two main tools: an in-house developed whole plant system code, pyTok [4], and the ASTRA-SPIDER code [5–7]. PyTok generates a self-consistent list of high-level tokamak design parameters based on a set of input assumptions and in addition estimates the construction cost and cost of electricity based on the fusion power produced. It includes simplified models for all major plant systems: HTS magnets, plasma, power cycle, shielding, Grad-Shafranov equilibrium, exhaust, costing, fuel cycle. It allows for the large parameter space optimisation and sensitivity studies, and generates free-boundary equilibrium.

First, main assumptions, targets, and constraints are defined. From the HCD point of view, all scenarios assume the fully non-inductive CD approach during flat-top phase. Then assumptions are given to pyTok, which identifies a

*Corresponding author: aleksandra.alieva@tokamakenergy.com

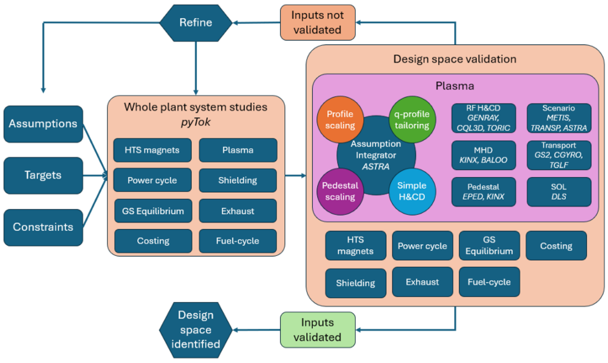

Figure 1. Scheme of the integrated modelling workflow.

Table 1. Design parameters.

Parameter	Lower A	Medium A	Higher A
R_{geo} [m]	4.25	4.25	4.25
B_T [T]	3.0	4.25	4.9
A	1.85	2.0	2.1
P_{fus} [MW]	730	825	880
$P_{elec,\ net}$ [MWe]	60	85	100

promising region of design space and helps to investigate design trade-offs. A combination of several low fidelity models then are given to the ASTRA-SPIDER 1.5D, 1D transport code coupled with 2D equilibrium solver, which is used as an assumption integrator to develop consistent flat-top plasma operating points. It takes 0D system code outputs and generates 1D kinetic profiles and 2D plasma equilibrium for the further studies. If inputs are not validated then initial assumptions are refined and the iteration is repeated, otherwise the design space is identified.

Plasma designs used in this study were obtained under the investigation of the trade-off between magnetic field B_T and aspect ratio $A = R_{geo}/a$ (where R_{geo} is the geometrical major radius, which was kept identical for all designs, and a is the minor radius). Table 1 presents comparison for the given plasma designs. There are lower A, medium A, and higher A plasmas with $A = [1.85,\ 2.0,\ 2.1]$, respectively. These designs provide different fusion powers and as a consequence the net electric powers, which meet the requirement of the project.

The HCD requirements for the current ramp-up phase are beyond the scope of this study, but some preliminary ideas have been presented in the work [8]. For the flat-top phase, the ECCD method was chosen as the only auxiliary HCD source, for the reasons outlined in the introduction. Figure 2 compares the plasma profile parameters received using the ASTRA-SPIDER code for given designs. The normalised coordinate is defined as the normalised poloidal flux $\rho = \frac{\Psi - \Psi_0}{\Psi_{LCFS} - \Psi_0}$, where Ψ is the poloidal magnetic flux, Ψ_0 is the poloidal magnetic flux on the magnetic axis, and Ψ_{LCFS} is the poloidal magnetic flux on the last closed flux surface. The electron density n_e is the same for all plasmas, the central value is $n_{e0} \approx 1.02 \times 10^{20}$ m^{-3}. However, the electron temperature T_e and current density

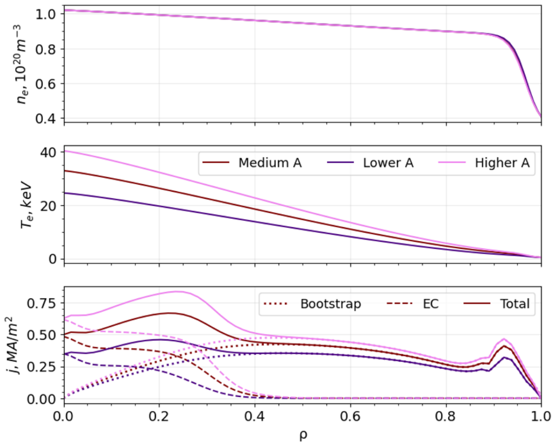

Figure 2. Electron density n_e, electron temperature T_e, and plasma current profiles as a function of normalised poloidal flux ρ for three plasma designs.

j profiles are different. The central electron temperature $T_{e0} \approx [24,\ 32,\ 40]$ keV for the lower, medium, and higher A designs, respectively. The last part illustrates current density profiles, which consist of a bootstrap fraction and an EC driven fraction. The latter is responsible for the on-axis and core CD, while bootstrap provides the CD along all plasma radii. These plasma profiles lead to design points targeting necessary net electric power $P_{elec,\ net}$ and overnight capital cost.

3 ECCD parametric scan

The ray-tracing code GENRAY [9] was used to perform a parametric scan in a wide range of frequencies for the given FPP designs. As previously mentioned in the introduction, the parameter of interest is the dimensionless current drive efficiency [10]:

$$\zeta_{ECCD} = 32.7 \frac{R_{geo} n_e [\times 10^{20} m^{-3}] I_{EC}[A]}{T_e[keV] P_{EC}[W]}, \qquad (1)$$

where I_{EC} is a driven current by the injected power P_{EC}.

Here the goal was to build a sufficient dataset and investigate trends to maximise the ζ_{ECCD}. For the present work, the Lin-Liu's current drive routine [11] with momentum conservation in electron-electron collisions had been chosen. The following parameters were varied: coordinate (radius R, height Z); toroidal ϕ and poloidal θ angles of wave launch with 10°step; wave frequency with 5 GHz step; two wave polarisations, ordinary O mode and extraordinary X mode. However, the influence of the effective charge on the ECCD was not investigated for the scan itself, and $Z_{eff} = 2.2$ was kept constant. Additionally, for faster evaluation, the single-ray approach was used. The scanned starting locations for ray launch surrounding the plasma from both sides is shown in figure 3, the bold contour indicates the last closed flux surface.

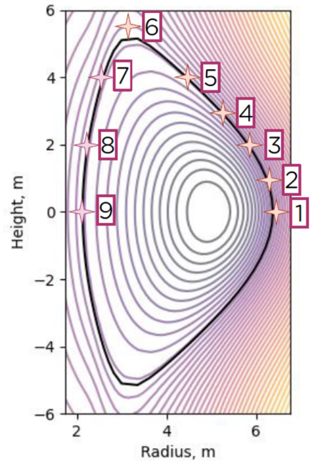

Figure 3. An example of launcher locations around the plasma edge for the medium A design.

The criterion of frequency choice is limited by the accessibility region for a given density and magnetic field profiles. For the cold plasma case, figure 4 shows the midplane locations of the fundamental resonance ω_{ce} and its 2^{nd} and 3^{rd} harmonics, $2\omega_{ce}$ and $3\omega_{ce}$, respectively; the upper hybrid resonance ω_{UH}; the plasma frequency ω_{pe}; and the X-mode cut-offs ω_{LH} and ω_{RH}. For all three designs, the fundamental harmonic X1 mode is not accessible from the low field side (LFS) launch, while it still can propagate from the high field side (HFS). Moreover, for the lower A design there is a region where the 2^{nd} harmonic X2 mode is covered by the cut-off, while the 3^{rd} harmonic X3 mode starts to play a role. For this design, the fundamental O1 mode is also partially covered by the plasma frequency and for low frequencies available for a radius less than $R < 3.9$ m, while for other designs it is mostly accessible for given radial positions and frequencies. The 2^{nd} harmonic O2 mode (and all higher harmonics) is accessible for all designs and radii. Thus, scans were performed for frequencies around $f = 90 - 220$ GHz.

4 Results and discussion

The ECCD efficiency for the medium A design is presented as an example of obtained results. Figure 5a shows the comparison of ζ_{ECCD} obtained for the O and X modes, LFS launch for a fixed midplane location (R, Z). Figure 5b shows the comparison of ζ_{ECCD} obtained for the O mode, LFS and HFS launchers. Every point in both figures represents a data point from the scanned set of injection angles and frequencies. It should be noted that simulations account for the absorption from all resonance harmonic layers with which the propagating wave interacts.

According to the current density j profiles provided (see figure 2), ECCD should be significant in plasma regions up to $\rho = 0.4$. These results of the scan demonstrate two things. Firstly, figure 5a illustrates that the O mode can provide ECCD along all plasma radii, while the X mode starts to play a role only in the off-axis regions. This happens because a wave is highly absorbed at the

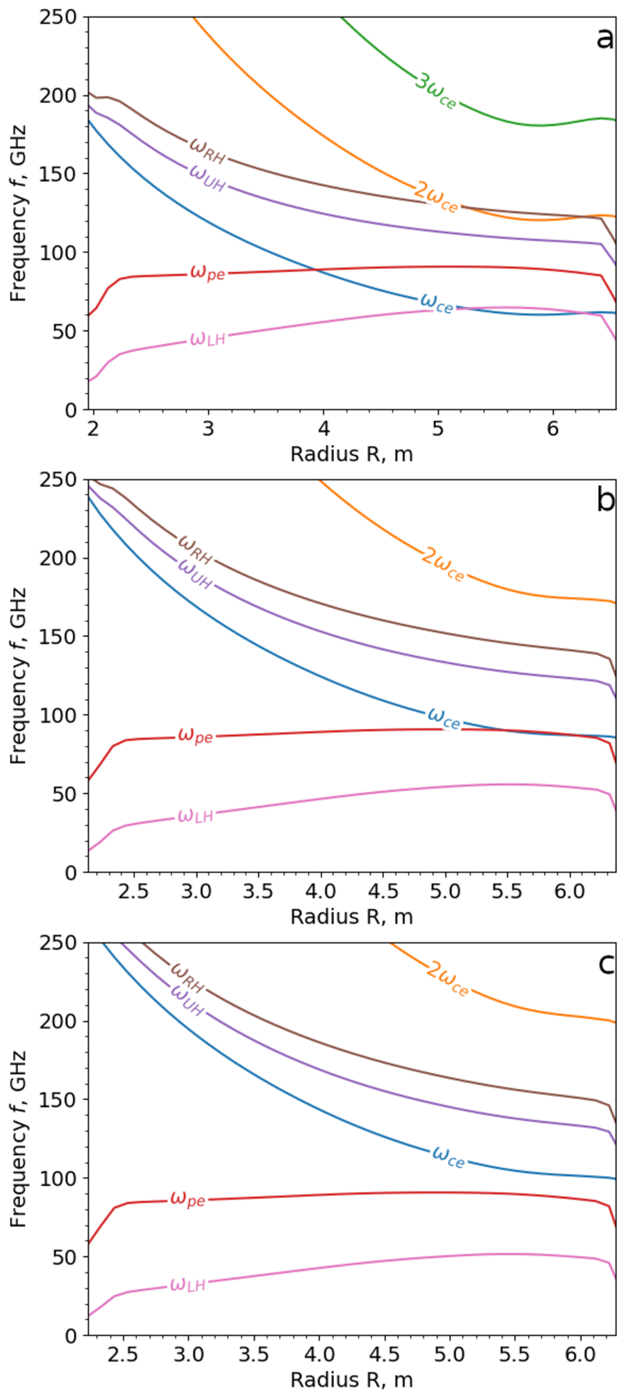

Figure 4. Resonances and cut-offs positions as a functions of radius along the midplane for given plasmas: a) lower A design, b) medium A design, c) higher A design.

Doppler-broaden X2 resonance layer and X1 is under cut-off, achieving central X2 absorption would require higher frequencies $f > 220$ GHz.

Secondly, even the O mode waves launched from the HFS cannot provide current generation in the region of interest (figure 5b). An absorption is shifted to the regions of higher ρ in addition to the fact that the parallel field refractive index $N_{\parallel} = k_{\parallel}c/\omega$ (where $k_{\parallel}$ is the parallel wave vector, c is the speed of light) is not optimal enough for current drive. The X1 mode launched from the HFS is highly

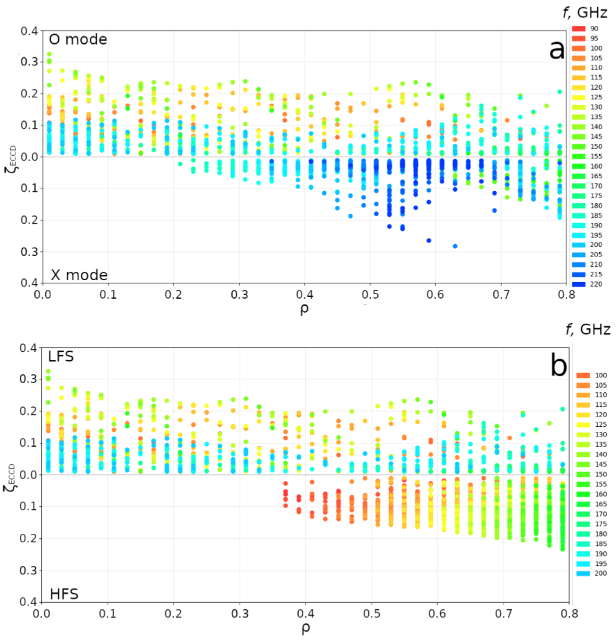

Figure 5. Dimensionless CD efficiency as a function of normalised poloidal flux for medium A design: a) comparison between O mode and X mode, b) comparison between LFS and HFS O mode.

absorbed[1]. Consequently, no ECCD was observed in the plasma core. Besides, limitations on the HFS launch are placed by the small inner space of the tokamak, where the central solenoid and inboard legs of the toroidal field coils have to be placed. Therefore, the O mode wave launched from positions (1 − 6) in figure 3 is considered optimal providing $\zeta_{ECCD} \approx 0.3$ throughout almost all plasma radii for all designs. Note that these general conclusions are consistent with what have been reported in other reactor studies [12, 13]

Consider figures 6, 7, 8 which show ζ_{ECCD} as a function of frequencies and normalised poloidal flux ρ for different launcher locations for the O mode for lower, medium, and higher A designs, respectively. This dataset depicts the best CD efficiencies among all scans at the chosen location (R, Z) for the O mode. The region of interest is still $\rho \leq 0.4$ but for a broader picture results up to $\rho = 0.8$ are shown.

Lower A design. Only moderate ECCD efficiencies have been yielded for this plasma design. The highest $\zeta_{ECCD} \approx 0.3$ has been reached for launcher (5) at $\rho = 0.4 - 0.5$, which does not satisfy the requested position. Simultaneously, the top launcher (6) does not produce any reasonable ζ_{ECCD} at all. The performance of the remaining launchers is not adequate enough, providing $\zeta_{ECCD} \approx 0.15 - 0.25$. In figure 6 zones with increased ζ_{ECCD} are clearly seen as brighter regions: frequencies $f \approx 135 - 180$ GHz can provide some amount of CD for the on-axis radii due to O2 mode absorption, while at higher placed launchers (3 − 4) frequencies around $f \approx 100 - 120$ GHz are responsible for core and off-axis CD due to O1 mode absorption. O3 affects performance at $f \gtrsim 200$ GHz, which is not shown here. On the whole, at the required radii $\zeta_{ECCD} \approx 0.20 - 0.25$ for the launchers (2 − 4).

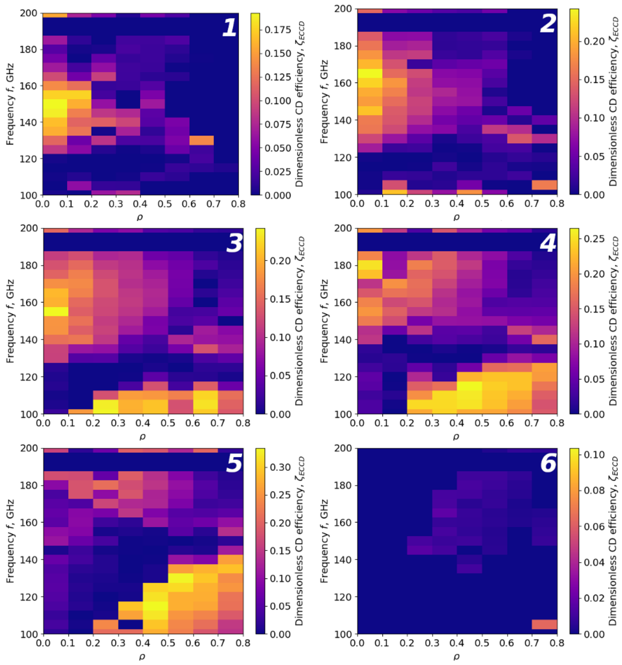

Figure 6. Dimensionless CD efficiencies as a function of frequency and major radius for different launchers from LFS for lower A: locations (1 − 6).

Medium A design. The results for the medium A plasma show the best CD efficiencies among all considered plasmas. The maximum $\zeta_{ECCD} \approx 0.35$ achieved for the off-axis radii, while for the region of interest it reaches $\zeta_{ECCD} \approx 0.3$. For the latter case, lower frequencies should be used for launchers (1 − 4), while launcher (5) at higher frequencies is more suitable for off-axis ECCD. Launcher 6 is limited again. For this plasma scenario, the fundamental harmonic is responsible for the wave absorption and current drive at given frequencies, thus, the higher ζ_{ECCD} is achieved.

Higher A design. The results for this plasma follow pattern similar to those observed for the medium A design. Near midplane launchers are suitable for the on-axis and core ECCD, while higher launchers are convenient for off-axis. Again, the top launcher does not provide any satisfactory results. In general, the efficiency of the ECCD is lower $\zeta_{ECCD} \approx 0.25$ compared to that of the medium A plasma. This limitation is due to the higher plasma temperatures, which cause a wider Doppler broadening, increasing the influence of the O2 mode.

For medium and higher A designs it is clearly seen that a higher ζ_{ECCD} for on-axis are achievable for closer to the midplane launchers at lower frequencies. For the outer radius launchers located closer to the top at higher frequencies are used to prevent an effect of trapped particles on ECCD efficiency [13]. The lower A design does not give

[1]This fact also prevents the use of electron Bernstein waves (EBWs) during the flat-top phase of operation, which could only possibly be excited via direct HFS X-B mode conversion due to the relatively low density of the candidate design points.

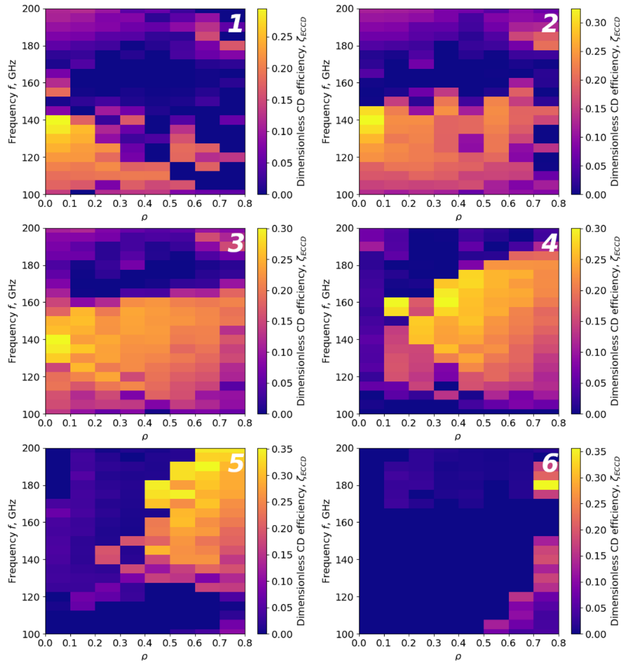

Figure 7. Dimensionless CD efficiencies as a function of frequency and major radius for different launchers from LFS for medium A: locations (1 – 6).

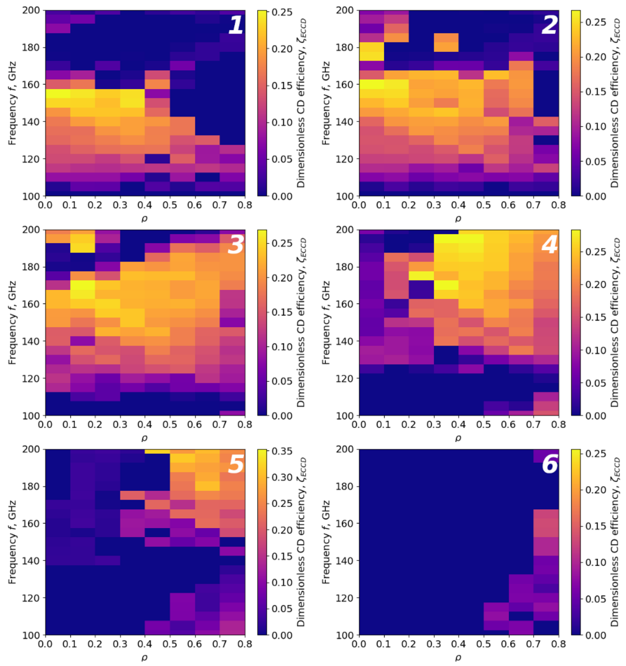

Figure 8. Dimensionless CD efficiencies as a function of frequency and major radius for different launchers from LFS for higher A: locations (1 – 6).

such effect for the considered range of frequencies due to the presence of the higher harmonic layers, which reduce the overall CD efficiency. Hence, optimal core ECCD is the O mode LFS midplane launch with $f = 125 - 145$ GHz, optimal frequencies are higher than cold resonance ones due to the Doppler shift [13]. Optimal edge ECCD is the top launch of O mode with $f = 160 - 200$ GHz.

By means of the raw CD efficiencies the values are around $\frac{I_{EC}}{P_{EC}} \approx 70 - 75\,\frac{\text{kA}}{\text{MW}}$, decreasing to $\frac{I_{EC}}{P_{EC}} \approx 40 - 50\frac{\text{kA}}{\text{MW}}$ while going to $\rho = 0.4$. Similar results were obtained using fast physics optimisation [14] based on the HARE module [15]. For the lower A plasma, the raw CD efficiency reaches only $\frac{I_{EC}}{P_{EC}} \approx 40\,\frac{\text{kA}}{\text{MW}}$ on-axis.

For the medium A design, a simple sensitivity study was also performed to extract the dependence of ζ_{ECCD} on Z_{eff} by also performing simulations with $Z_{eff} = 1$ for select, best-performing launchers. The resulting improvement in ECCD efficiency at low Z_{eff} is well described by a dependence $\zeta_{ECCD} \propto \frac{1}{2.3+Z_{eff}}$. Although this conclusion is based on an admittedly small sample set, it is consistent with the Z_{eff} dependence inferred in STEP simulations [12].

5 Conclusion

In this study the ECCD launcher optimization was performed by means of a large parametric scan over a set of parameters (launcher positions (R, Z), frequencies, injection angles, and wave polarisation) for 3 proposed preconceptual designs of TE FPP using the ray-tracing code GENRAY. The location of the launcher and the choice of frequency have a large effect on the ECCD performance. On the one hand, for designs with an aspect ratio $A = [2.0,\ 2.1]$ if the ECCD has to be on-axis and at the core, it is necessary to choose locations on or around the midplane, launchers (1 – 4), using lower range frequencies. For the efficient ECCD in the off-axis region, higher frequencies for launcher 5 should be considered. On the other hand, this trend is not followed for the design with $A = 1.85$. The presence of the O2 harmonic results in a large reduction in the ECCD performance. Exclusion of the O2 mode from the plasma region by the frequencies is limited because here the O1 mode is below the cut-off for the given magnetic field and plasma profiles.

Overall, the results obtained showed that normalised ECCD efficiency $\zeta_{ECCD} \approx 0.3$ across the plasma radius can be achieved for the O mode LFS and top launchers for the medium A design. Other plasma designs showed less efficient results because of the influence of the higher harmonic presence. The findings of this study have subsequently been used to develop a fast physics-based optimization of ECCD launchers [14], and have continued to inform the HCD considerations during the ongoing progression of the TE FPP design project.

Acknowledgement

Tokamak Energy acknowledges U.S. Federal support for this work under TIA DE-SC002488.

This work was prepared under an agreement with and funded by the U.S. Government. Neither the U. S. Government or its employees, nor any of its contractors, subcontractors or their employees, makes any express or implied:

1. warranty or assumes any legal liability for the accuracy, completeness, or for the use or results of such use of any information, product, or process disclosed; or

2. representation that such use or results of such use would not infringe privately owned rights; or

3. endorsement or recommendation of any specifically identified commercial product, process, or service. Any views and opinions of authors expressed in this work do not necessarily state or reflect those of the United States Government, its contractors or subcontractors.

References

[1] https://www.energy.gov/

[2] D. Kingham, M. Gryaznevich. The spherical tokamak path to fusion power: Opportunities and challenges for development via public–private partnerships. Phys. Plasmas **31**, 042507 (2024). https://doi.org/10.1063/5.0170088

[3] V. Erckmann, U. Gasparino. Electron cyclotron resonance heating and current drive in toroidal fusion plasmas. Plasma Phys. Control. Fusion **36**, 1869 (1994). https://doi.org/10.1088/0741-3335/36/12/001

[4] E. Maartensson, S. McNamara. Early design workflow and progress of Tokamak Energy's high-field spherical tokamak fusion pilot plant for the US DOE Milestone-Based Fusion Development Program, 66th Annual Meeting of the APS Division of Plasma Physics, Atlanta, USA, October 7–11 (2024).

[5] A. Dnestrovskiy et al. Application of modified ASTRA-SPIDER code to simulation of free boundary equilibrium evolution. In 45th EPS Conference on Plasma Physics, EPS 2018, pp. 1212-1215, (2018). https://info.fusion.ciemat.es/OCS/EPS2018ABS/pdf/P4.1080.pdf

[6] G. V. Pereverzev, E. P. Yushmanov, ASTRA. Automated System for TRansport Analysis in a tokamak, IPP 5/98, Garching: Max-Planck-Institut für Plasmaphysik (2002). https://hdl.handle.net/11858/00-001M-0000-0027-4510-D

[7] A. A. Ivanov, et al. New adaptive grid plasma evolution code SPIDER, 32nd EPS Conference on Plasma Phys., ECA, Vol. **29**, pp. 5-063 (2005). https://info.fusion.ciemat.es/OCS/EPS2005/pdf/P5_063.pdf

[8] Y. Takase, et al. Ramp-up and sustainment scenarios for Tokamak Energy's Fusion Pilot Plan, 25th Topical Conference on Radio-Frequency Power in Plasmas, Schloss Hohenkammer, Germany, May 19-22 (2025). https://www.ipp.mpg.de/5487515/Talks

[9] A. P. Smirnov, R. W. Harvey. The GENRAY ray tracing code, CompX Report CompX-2000-01, (2001). https://piscope1.psfc.mit.edu/images/2/21/Genray_manual_CompX-2001-1-V2.pdf

[10] T. C. Luce, et al. Generation of localized noninductive current by electron cyclotron waves on the DIII-D tokamak. Phys. Rev. Lett. **83**, 4550 (1999). https://doi.org/10.1103/PhysRevLett.83.4550

[11] Y. R. Lin-Liu, et al. Electron cyclotron current drive efficiency in general tokamak geometry. Phys. Plasmas **10**, 4064–4071 (2003). https://doi.org/10.1063/1.1610472

[12] S. Freethy, et al. The optimisation of the STEP electron cyclotron current drive concept. Nucl. Fusion **64**, 126035 (2024). https://doi.org/10.1088/1741-4326/ad7a8a

[13] E. Poli, et al. Electron-cyclotron-current-drive efficiency in DEMO plasmas. Nucl. Fusion **53**, 013011 (2013). https://doi.org/10.1088/0029-5515/53/1/013011

[14] N. A. Lopez, et al. Fast physics-based launcher optimization for electron cyclotron current drive. Plasma Phys. Control. Fusion **67**, 055012 (2025). https://doi.org/10.1088/1361-6587/adcae7

[15] E. Poli, et al. Fast evaluation of the current driven by electron cyclotron waves for reactor studies. Phys. Plasmas **25**, 122501 (2018). https://doi.org/10.1063/1.5050345